Shear instability of a planar liquid jet immersed in a high speed gas stream

by Juan C. Padrino (Advisor: D.D. Joseph)
2/4/06 2:46 AM

Consider a planar liquid jet surrounded by a high speed gas stream. Following the work of Raynal, Villermaux, Lasheras & Hopfinger (1997), Villermaux (1998a) and Varga, Lasheras & Hopfinger (2003), the corresponding basic flow can be idealized by a piecewise linear velocity profile such that the liquid jet velocity is U_1 and the gas velocity is U_2, with $U_2 > U_1$. The continuity of the basic velocity profile is represented by a linear transition region completely contained in the gas with thickness δ (Figure 1 a). An observer moving with the average velocity $U_{avg} = (U_1 + U_2)/2$ parallel to the basic flow identifies a piecewise linear velocity profile as shown in Figure 1 b with $U_0 = (U_2-U_1)/2$. By making use of a Galilean transformation, the stability analysis is performed under a reference frame moving with U_{avg} without loss of generality.

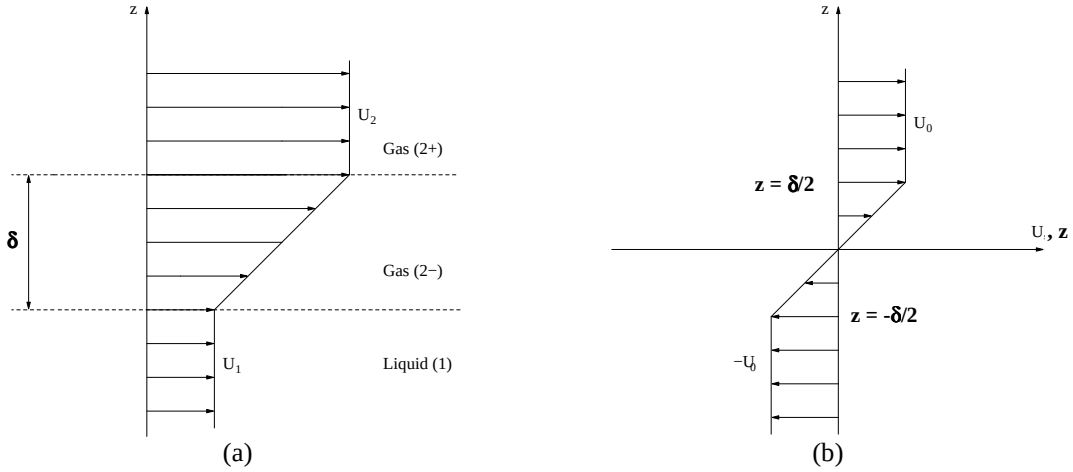

Figure 1 Sketch of the piecewise velocity profile for the gas-liquid shear layer: (a) observer at rest; (b) observer moving with velocity $U_{avg} = (U_1+U_2)/2$ parallel to the main flow.

The laminar basic flow for the piecewise linear profile is described as follows,

$$U(z) = \begin{cases} U_0, & z > \delta/2 \\ \dfrac{2U_0}{\delta} z & -\delta/2 < z < \delta/2 \\ -U_0, & z < -\delta/2 \end{cases} \qquad (1)$$

where, z is the Cartesian coordinate along the direction normal to the basic flow. In the analysis that follows the gas and liquid are regarded as incompressible. The density and dynamic viscosity of the liquid phase are ρ_1 and μ_1, respectively, while, the gas density

and dynamic viscosity are designated as ρ_2 and μ_2, correspondingly. Therefore, the density profile is defined as $\rho = \rho_2$ for $z > -\delta/2$ and $\rho = \rho_1$ for $z < -\delta/2$, whereas the dynamic viscosity profile is given by $\mu = \mu_2$ for $z > -\delta/2$ and $\mu = \mu_1$ for $z < -\delta/2$. The surface tension is denoted by γ; $P = P(z)$ is the undisturbed pressure.

Consider small disturbances of the basic velocity and pressure fields u', v', w' and p', such that the disturbed flow motion is

$$\begin{aligned} u &= U + u', \\ v &= v', \\ w &= w', \\ p &= P + p'. \end{aligned} \tag{2}$$

For the basic or undisturbed fluid motion two "interfaces" are set: A virtual "interface" at $z = \delta/2$, since the gas phase is in both sides, and the actual interface at $z = -\delta/2$, with the gas stream above and the liquid phase below. The disturbed flow introduce small perturbations of these interfaces, which are modeled as

$$z = \delta/2 + \zeta(x, y, t),$$

and

$$z = -\delta/2 + \xi(x, y, t), \tag{3}$$

for the top and bottom interfaces, respectively ($\zeta << \delta/2$ and $\xi << \delta/2$).

The standard linear stability analysis follows with the substitution of (2) into the incompressible unsteady Navier –Stokes equations, neglecting products of the disturbances and their derivatives, which are considered "small" in comparison with the remaining terms. Then, the corresponding equations for the main or basic flow are substracted. Furthermore, we assume, for simplicity, that the disturbance of the velocity field is irrotational, such that $\nabla^2 \mathbf{u}' = 0$. The irrotational character of the disturbance is enforced even though the basic fluid motion clearly has non-zero vorticity in the layer $-\delta/2 \le z \le \delta/2$ (Figure 1). We end up with the following system of linear partial differential equations:

$$\begin{aligned} \frac{\partial u'}{\partial t} + U\frac{\partial u'}{\partial x} + w'\frac{\partial U}{\partial z} &= -\frac{1}{\rho}\frac{\partial p'}{\partial x}, \\ \frac{\partial v'}{\partial t} + U\frac{\partial v'}{\partial x} &= -\frac{1}{\rho}\frac{\partial p'}{\partial y}, \end{aligned} \tag{4}$$

$$\frac{\partial w'}{\partial t}+U\frac{\partial w'}{\partial x}=-\frac{1}{\rho}\frac{\partial p'}{\partial z},$$

$$\frac{\partial u'}{\partial x}+\frac{\partial v'}{\partial y}+\frac{\partial w'}{\partial z}=0,$$

which governs the linear stability problem in the three regions $z>\delta/2+\zeta$, $-\delta/2+\xi<z<\delta/2+\zeta$ and $z<-\delta/2+\xi$.

Notice that the viscous terms have vanished in the resulting system of equations (4). However, we have not assumed that the fluids are inviscid. What we did presuppose is that the small disturbances are irrotational. In fact, the viscosity of the fluid will enter the problem through the balance of the normal stresses. This provision is the main postulate of the viscous potential flow analysis (references here). In other words, the disturbance of the basic fluid motion is regarded as irrotational flow of a viscous fluid. Inviscid stability analysis of the piecewise linear velocity profile for a single phase flow have been performed by Rayleigh (1894), Drazin and Reid (1961) and recently by Criminale, Jackson and Joslin (2003), among others. Changes in the density along the normal direction are included in the inviscid analysis presented by Chandrasekhar (1961). The steps outlined by this author in its comprehensive study of the shear stability for the piecewise linear profile are followed here with the corresponding modifications that stem from viscous potential flow and the addition of surface tension's contribution.

The boundary conditions requires that the disturbances must vanish as $z\to\pm\infty$. Moreover, at the interfaces $z=\delta/2+\zeta$ and $z=-\delta/2+\xi$, the jump of the normal stress across the interface is balance by the surface tension γ. This condition can be written as

$$\left\langle -p+2\mu\mathbf{n}\cdot\nabla\mathbf{u}\cdot\mathbf{n}\right\rangle=-\gamma\nabla\cdot\mathbf{n}, \tag{5}$$

where $\mathbf{n}$ is the outward normal unit vector from the liquid at the gas-liquid interface. The notation $\langle\cdot\rangle=(\cdot)\big|_{z=a^+}-(\cdot)\big|_{z=a^-}$ has been used to indicate the jump across the interface defined by $z=a$. Clearly, for $z=\delta/2+\zeta$ the jump in the normal stress is zero, since a gas-liquid interface exists only at $z=-\delta/2+\xi$. Substitution of (2) into (5) yields expressions for the boundary conditions at $z=\delta/2+\zeta$ and $z=-\delta/2+\xi$. For the piecewise linear profile, we cannot impose the continuity of the tangential stress.

In addition, two kinematics conditions can be prescribed at the "interfaces"

$$w'=\frac{D\zeta}{Dt}=\frac{\partial\zeta}{\partial t}+\mathbf{u}\cdot\nabla\zeta, \qquad \text{at } z=\delta/2+\zeta \tag{6}$$

$$w'=\frac{D\xi}{Dt}=\frac{\partial\xi}{\partial t}+\mathbf{u}\cdot\nabla\xi, \qquad \text{at } z=-\delta/2+\xi \tag{7}$$

The boundary conditions (5), (6) and (7) can also be linearized for small disturbances yielding,

$$p'_{2^-} - p'_{2^+} + 2\mu_2 \left[\left(\frac{\partial w'}{\partial z} \right)_{2^+} - \left(\frac{\partial w'}{\partial z} \right)_{2^-} \right] + 2\mu_2 \left(\frac{\partial \zeta}{\partial x} \frac{\partial U}{\partial z} \right)_{2^-} = 0, \qquad \text{at } z = \delta/2, \tag{8}$$

and

$$p'_1 - p'_{2^-} - (\rho_1 - \rho_2) g \xi + 2\mu_2 \left(\frac{\partial w'}{\partial z} - \frac{\partial \xi}{\partial x} \frac{\partial U}{\partial z} \right)_{2^-} - 2\mu_1 \left(\frac{\partial w'}{\partial z} \right)_1 = -\gamma \left(\frac{\partial^2 \xi}{\partial x^2} + \frac{\partial^2 \xi}{\partial y^2} \right), \tag{9}$$

$$\text{at } z = -\delta/2,$$

for the normal stress balance and,

$$w' = \frac{\partial \zeta}{\partial t} + U \frac{\partial \zeta}{\partial x}, \qquad \text{at } z = \delta/2, \tag{10}$$

$$w' = \frac{\partial \xi}{\partial t} + U \frac{\partial \xi}{\partial x}, \qquad \text{at } z = -\delta/2, \tag{11}$$

for the kinematic conditions. Therefore, the problem of linear stability analysis of a gas-liquid shear layer described by a piecewise linear profile using the viscous potential flow approach is posed by the system of equations (4) with boundary conditions (8) through (11), with disturbances vanishing at $z \to \pm\infty$. Notice also that the factor $\partial U / \partial z = 0$ for $z > \delta/2$ and $z < -\delta/2$ according to (1).

Since the problem is defined by perturbations of a parallel flow, we can assume normal modes solutions of the type

$$\begin{aligned}
u'(x,y,z,t) &= \frac{1}{2}(\hat{u}(z) e^{i(kx+ly+\omega t)} + c.c.), \\
v'(x,y,z,t) &= \frac{1}{2}(\hat{v}(z) e^{i(kx+ly+\omega t)} + c.c.), \\
w'(x,y,z,t) &= \frac{1}{2}(\hat{w}(z) e^{i(kx+ly+\omega t)} + c.c.), \\
p'(x,y,z,t) &= \frac{1}{2}(\hat{p}(z) e^{i(kx+ly+\omega t)} + c.c.), \\
\zeta(x,y,t) &= \frac{1}{2}(\hat{\zeta} e^{i(kx+ly+\omega t)} + c.c.),
\end{aligned} \tag{12}$$

$$\xi(x,y,t) = \frac{1}{2}(\hat{\xi} e^{i(kx+ly+\omega t)} + c.c.),$$

where *c.c.* stands for the complex conjugate of the previous term in parenthesis. The constants $\hat{\zeta} << \delta/2$ and $\hat{\xi} << \delta/2$. These normal modes allow the reduction of the system of partial differential equations to a system of ordinary differential equations. In this study, we endeavor to the temporal stability analysis. Therefore, the wavenumbers in the *x* and *y* directions, *k* and *l*, respectively, are enforced to be real whereas the frequency of the disturbance ω is allowed to be complex.

Substitution of (12) into (4) yields, after some algebraic manipulation, to an ordinary differential equation for $\hat{w}$,

$$\frac{d^2\hat{w}}{dz^2} - \hat{k}^2\hat{w} = 0, \tag{13}$$

with solutions,

$$\hat{w}(z) = Ae^{\hat{k}z} + Be^{-\hat{k}z}, \tag{14}$$

with $\hat{k} = \sqrt{k^2 + l^2}$. Therefore, for the three regions of the domain we end up with the following system

$$\begin{aligned}
&\hat{w} = A_{2^+} e^{-\hat{k}z}, && \text{for } z > \delta/2, \\
&\hat{w} = A_{2^-} e^{\hat{k}z} + B_{2^-} e^{-\hat{k}z}, && \text{for } -\delta/2 < z < \delta/2, \\
&\hat{w} = B_1 e^{\hat{k}z}, && \text{for } z < -\delta/2,
\end{aligned} \tag{15}$$

satisfying the far field conditions at $z \to \pm\infty$.

Substitution of the normal modes (12) and the solution for $\hat{w}$ given in (15) into the boundary conditions for $z = \pm\delta/2$ (8) trough (11), determines the dispersion relation for the eigenvalue ω. Hereafter, by invoking the Squire's theorem (1933), it is assumed that the wavenumber *l* = 0. This theorem states that "to each unstable three-dimensional disturbance there corresponds a more unstable two-dimensional disturbance" (Criminale *et al*., 2003). In convenient dimensionless form, the resulting dispersion relation can be written as

$$e^{-2\eta} = \left[1 + (\Omega - \eta)\right]\left[\frac{\Phi + (\Omega+\eta)\left\{2\hat{\rho} - (1+\hat{\rho})(\Omega+\eta) - (1+\hat{\mu})\beta_1\eta^2\right\}}{\Phi + (\Omega+\eta)\left\{2\hat{\rho} - (1-\hat{\rho})(\Omega+\eta) - (1-\hat{\mu})\beta_1\eta^2\right\}}\right], \tag{16}$$

with,

$$\Phi = J_1\eta + \left(\frac{\hat{\rho}}{We_2}\right)\eta^3 + 2\eta^2\hat{\mu}\beta_1, \qquad \beta_1 = \frac{i2}{\mathrm{Re}_1} \tag{17}$$

and $i = \sqrt{-1}$. The numbers Ω and η are the dimensionless complex frequency of the disturbances and the dimensionless wavenumber, respectively, defined as

$$\Omega = -\frac{\omega\delta}{U_0} \qquad \text{and} \qquad \eta = k\delta. \tag{18}$$

The normal modes have been taken as $e^{i(kx+\omega t)}$ and Squire's theorem has been invoked. Expanding $\Omega = \Omega_r + i\Omega_i$, since ω is complex, temporal instability takes place when $\Omega_i > 0$. The density and viscosity ratios $\hat{\rho}$ and $\hat{\mu}$ are prescribed as

$$\hat{\rho} = \frac{\rho_2}{\rho_1} \qquad \text{and} \qquad \hat{\mu} = \frac{\mu_2}{\mu_1}. \tag{19}$$

Re_1 represents a Reynolds number based on the liquid properties; We_2 is the Weber number, which weighs surface tension forces with gas inertia effects; finally, J_1 is the Richardson number, which weighs buoyancy (gravity) with liquid inertia effects. They are defined as follows,

$$Re_1 = \frac{U_0\delta}{\nu_1}, \qquad We_2 = \frac{\rho_2 U_0^2\delta}{\gamma} \qquad \text{and} \qquad J_1 = \frac{(\rho_1 - \rho_2)g\delta}{\rho_1 U_0^2}. \tag{20}$$

where $\nu_1 = \mu_1/\rho_1$ is the kinematic viscosity of the liquid. Therefore, dispersion relation (16) for the dimensionless eigenvalue Ω has the generic form

$$D_1(\Omega, \eta, \hat{\rho}, \hat{\mu}, Re_1, We_2, J_1) = 0, \tag{21}$$

A Reynolds number based on the inertia of phase 2 (gas) can also be defined,

$$Re_2 = \frac{U_0\delta}{\nu_2}, \qquad \text{such that} \qquad \mathrm{Re}_1 = \frac{\hat{\mu}}{\hat{\rho}}Re_2, \tag{22}$$

and, then, the eigenvalue relation (21) can be redefined as

$$D_2(\Omega, \eta, \hat{\rho}, \hat{\mu}, Re_2, We_2, J_1) = 0, \tag{23}$$

Therefore, by specifying $\hat{\rho}, \hat{\mu}$ and Re_2, the parameter Re_1 is already fixed. The dispersion relation (16) can be written as a cubic equation as follows,

$$a_3\hat{\Omega}^3 + a_2\hat{\Omega}^2 + a_1\hat{\Omega} + a_0 = 0, \tag{24}$$

with $\hat{\Omega} = \Omega + \eta$. The coefficients are defined as,

$$a_3 = -(1+\hat{\rho}), \tag{25}$$

$$a_2 = 2\hat{\rho} - (1+\hat{\mu})\beta_1\eta^2 - (1-2\eta)(1+\hat{\rho}) + (1-\hat{\rho})e^{-2\eta}, \tag{26}$$

$$a_1 = \Phi + (1-2\eta)\left[2\hat{\rho} - (1+\hat{\mu})\beta_1\eta^2\right] - \left[2\hat{\rho} - (1-\hat{\mu})\beta_1\eta^2\right]e^{-2\eta}, \tag{27}$$

$$a_0 = \left[(1-2\eta) - e^{-2\eta}\right]\Phi. \tag{28}$$

In the case of inviscid fluids, taking $\mu_1 \to 0$ and $\mu_2 \to 0$ in (16), and neglecting gravitational and surface tension effects ($J_1 \to 0$ and $We_2 \to \infty$) yields $\Phi \to 0$ and (16) reduces to

$$e^{-2\eta} = \left[1 + (\Omega - \eta)\right]\left[\frac{2\hat{\rho} - (1+\hat{\rho})(\Omega+\eta)}{2\hat{\rho} - (1-\hat{\rho})(\Omega+\eta)}\right], \tag{29}$$

for which (24) becomes a quadratic equation

$$a_2\hat{\Omega}^2 + a_1\hat{\Omega} + a_0 = 0, \tag{30}$$

with

$$a_2 = -(1+\hat{\rho}), \tag{31}$$

$$a_2 = 2\hat{\rho} - (1-2\eta)(1+\hat{\rho}) + (1-\hat{\rho})e^{-2\eta}, \tag{32}$$

$$a_1 = 2\hat{\rho}\left[(1-2\eta) - e^{-2\eta}\right]. \tag{33}$$

Expression (29) is the same dispersion relation obtained by Villermaux (1998a) and Marmottant & Villermaux (2004) with respect to a reference frame moving with the velocity $U_{avg} = (U_1+U_2)/2$. Notice that by considering fluids 1 and 2 to be the same fluid in (29), one can readily find the dispersion relation first obtained by Rayleigh (1894) and also discussed by Drazin & Reid (1981) and Criminale *et al*. (2003).

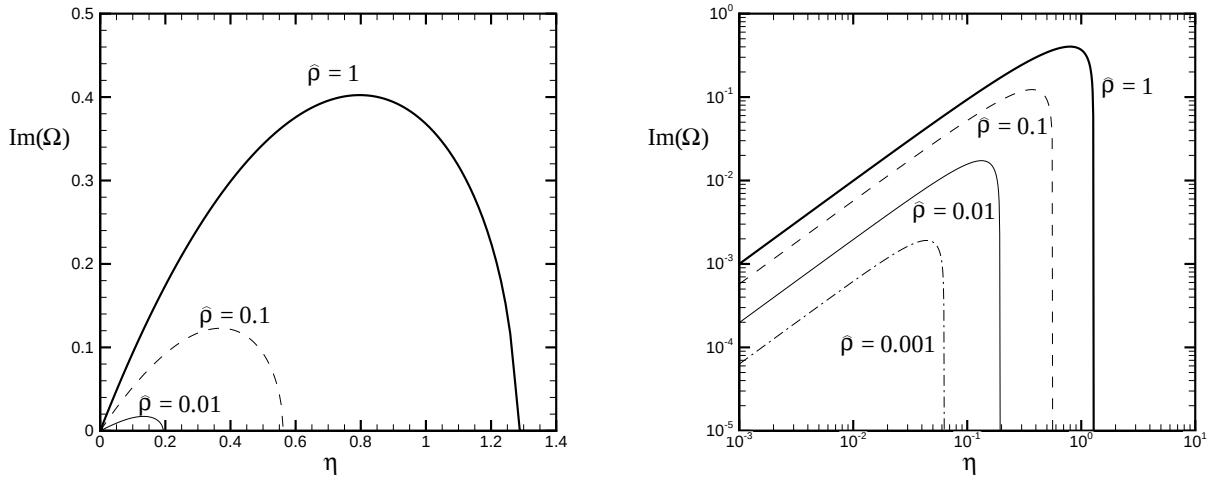

(a) Linear scale (b) Logarithm scale

Figure 2 Growth rate versus wavenumber (dimensionless) from inviscid potential flow for various density ratios $\hat{\rho}$: 0.001, 0.01, 0.1 and 1. Surface tension and gravitational effects are neglected (gas Weber number $We_2 \to \infty$ and Richardson number $J_1 = 0$). Our plots reproduce the results obtained by Villermaux (1998a). The dimensionless wavenumber is given by $\lambda / \delta = 2\pi / \eta$, where δ is the thickness of the vorticity layer in the basic flow (see Figure 1). The most dangerous wave is determined by the maximum value of Im(Ω).

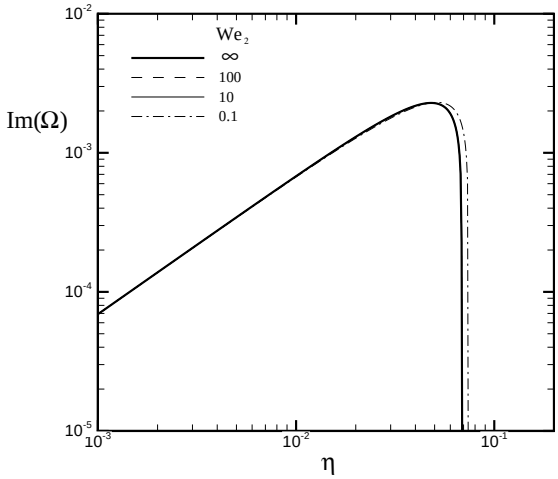

Figure 3 Growth rate versus wavenumber (dimensionless) from inviscid potential flow for a density ratio of $\hat{\rho}$ = 0.0012 (air-water) considering surface tension effects, for different values of the gas Weber number We_2, neglecting gravitational effects ($J_1 = 0$). The dimensionless wavenumber is given by $\lambda / \delta = 2\pi / \eta$, where δ is the thickness of the vorticity layer in the basic flow (see Figure 1). The most dangerous wave is determined by the maximum value of Im(Ω).

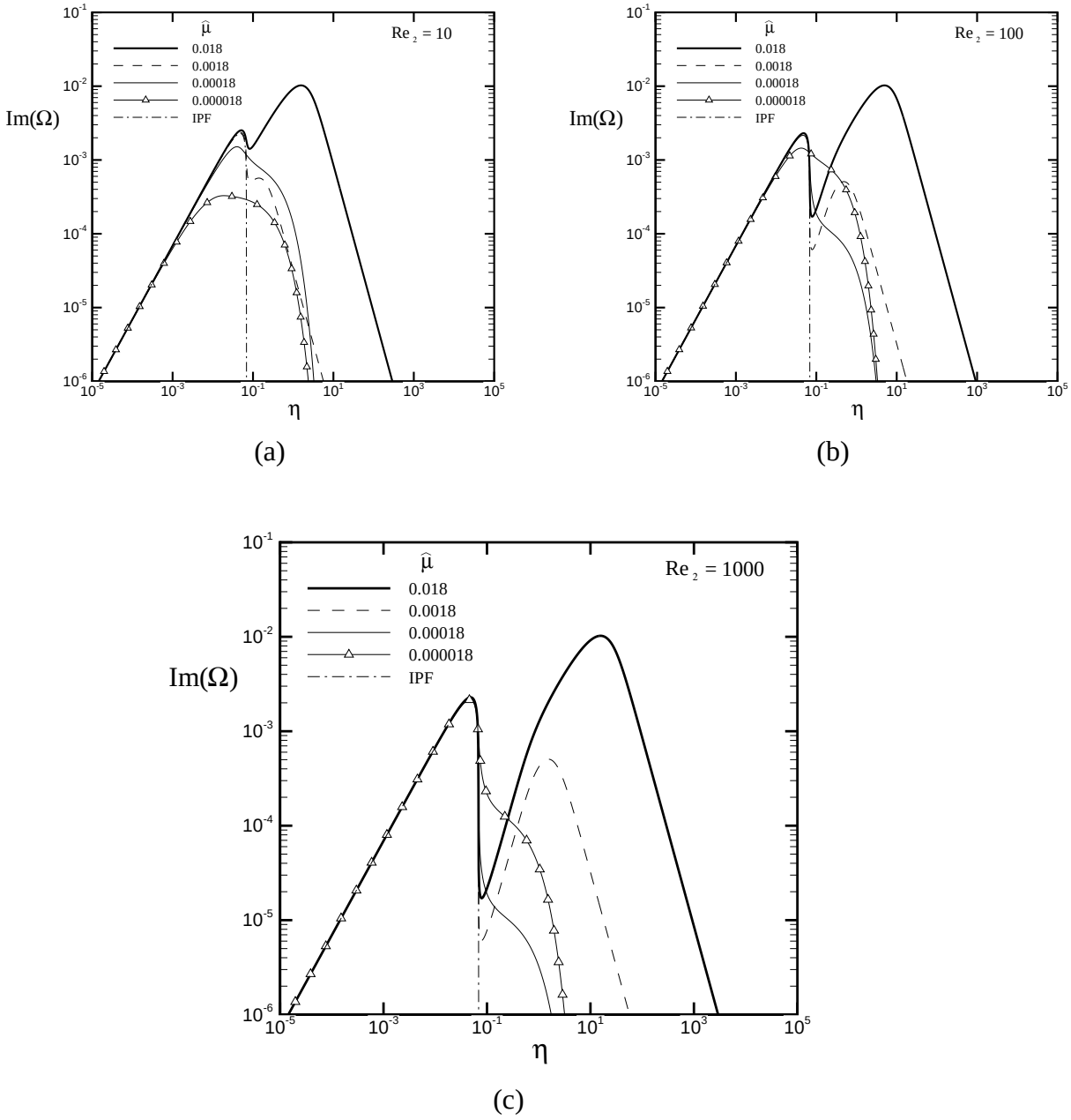

Figure 4 Growth rate versus wavenumber (dimensionless) from viscous potential flow for various viscosity ratios $\hat{\mu}$: 0.018 (air-water), 0.0018, 0.00018 and 0.000018, density ratio $\hat{\rho}$ = 0.0012 (air-water) and three different values of the gas Reynolds number Re_2: (a) 10, (b) 100 and (c) 1000. Surface tension and gravitational effects are neglected (gas Weber number $We_2 \to \infty$ and Richardson number $J_1 = 0$). The dimensionless wavenumber is given by $\lambda / \delta = 2\pi / \eta$, where δ is the thickness of the vorticity layer in the basic flow (see Figure 1). The most dangerous wave is determined by the maximum value of Im(Ω).

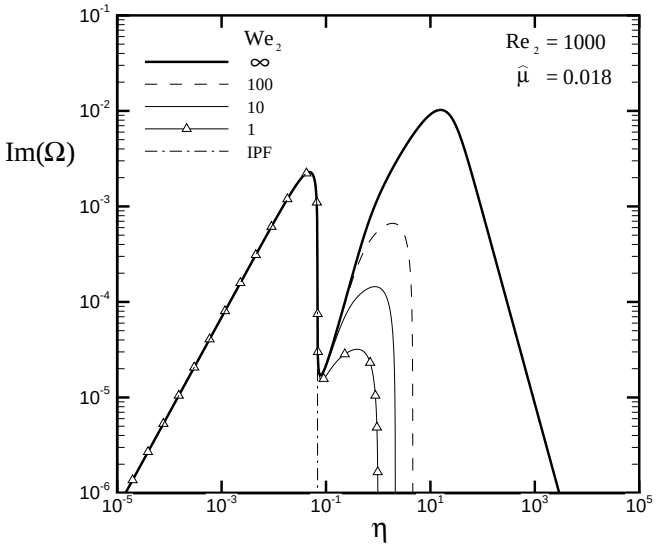

Figure 5 Growth rate versus wavenumber (dimensionless) from viscous potential flow for various We_2: 1, 10, 100 and ∞ for a gas Reynolds number $\mathrm{Re}_2 = 1000$, density ratio $\hat{\rho}$ = 0.0012 (air-water) and viscosity ratio $\hat{\mu}$ = 0.018 (air-water). Gravitational effects are neglected (Richardson number $J_1 = 0$). When surface tension is considered, the viscous mode (peak to the right) is overcome by the inviscid mode (peak to the left). For IPF (dash-dotted line), $We_2 \to \infty$. The dimensionless wavenumber is given by $\lambda / \delta = 2\pi / \eta$, where δ is the thickness of the vorticity layer in the basic flow (see Figure 1). The most dangerous wave is determined by the maximum value of Im(Ω). Examination of this plot suggests that if the wavelength of the most dangerous wave for air-water predicted by IPF is in agreement with experiments as indicated in the literature, then, when using VPF, surface tension effects cannot be neglected in order to obtain the correct trend. This conclusion is a consequence of the attenuation of the "viscous" mode (right peak in the spectrum) when decreasing the Weber number We_2, whereas the "inviscid" mode (left peak) remains essentially unperturbed.

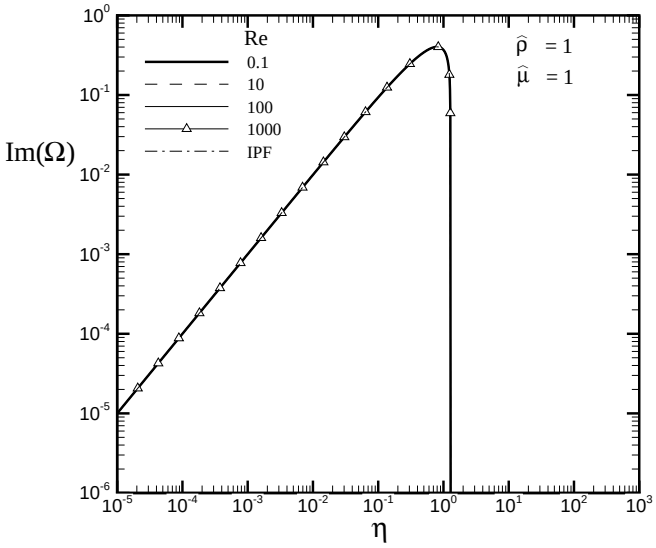

Figure 6 Growth rate versus wavenumber (dimensionless) from viscous potential flow for various Re: 0.1, 10, 100 and 1000 when both phases 1 and 2 corresponds to the same fluid. Obviously, neither gravitational effects nor surface tension effects enter the problem. For all Re, the curves collapse with the inviscid case! These results can be anticipated from Eq. (1) setting $\hat{\rho}$ = 1 and $\hat{\mu}$ =1 and comparing with the inviscid solution. The dimensionless wavenumber is given by $\lambda/\delta = 2\pi/\eta$, where δ is the thickness of the vorticity layer in the basic flow (see Figure 1). The most dangerous wave is determined by the maximum value of Im(Ω).

Comparison with experimental data

In this section we compare experimental results for the interface wave frequency *f* and the dimensionless wavelength λ/δ of the most amplified wave with predictions from the model described previously. The experimental data is taken from the literature and is divided in three sets depending upon the type of data measured (wave frequency or wavelength) and the gas-liquid configuration (planar or axisymmetric). The interface wave frequency *f* is the ratio of the convection velocity U_C to the distance between two consecutive structures λ,

$$f = \frac{U_c}{\lambda}, \tag{34}$$

or, expressed as a dimensionless number,

$$\frac{f\delta}{U_c} = \frac{\delta}{\lambda}, \tag{35}$$

which describes a Strouhal number for the passing of the waves. All the data sources considered provide an expression for the dependence of the vorticity thickness δ on the gas Reynolds number based on the thickness of the gas nozzle, which is linked with the shape and dimensions of the experimental set-up. Therefore, using the recorded frequencies and the thickness δ one can compute λ/δ from (35) if the convection velocity is known. In all the referred works, the convection velocity is expressed as (Bernal and Roshko 1986; Dimotakis 1986):

$$U_c = \frac{\sqrt{\rho_1}U_1 + \sqrt{\rho_2}U_2}{\sqrt{\rho_1} + \sqrt{\rho_2}}, \tag{36}$$

Table 1 summarizes some features of the experimental data. Set 1 refers to the wave frequency data by Raynal *et al*. (1997), for an air - water sheet system (planar situation). Set 2 considers the frequency data by Marmottant & Villermaux (2004) for a cylindrical liquid jet surrounded by a gas stream (axisymmetric configuration). Finally, Set 3 considers the wavelength data measured by Varga *et al*.(2003) and Marmottant & Villermaux (2004) for their axisymmetric configurations.

Table 2 presents the fluid properties used in the computations carried out in this investigation.

Marmottant & Villermaux have discussed some conditions for which the main assumptions of the model remains valid. The critical value Re_2 =50 establishes a threshold below which damping effects of viscosity starts to be important (Betchov & Szewczyk 1963; Villermaux 1998b). Almost the entire dataset in this investigation satisfies this condition. Furthermore, the adopted large vorticity layer description

remains valid in opposition to the thin vorticity layer characterized by a Kelvin-Helmholtz instability limit if the following condition is satisfied,

$$We_2\left(\frac{\rho_1}{\rho_2}\right)^{1/2} > 12.5, \tag{37}$$

For the data considered in this study, the average value of the dimensionless number in the L.H.S. of (37) is about 65 and 85% of the points satisfy this condition. Finally, in the case of the axisymmetric jet, capillary instability is overcome by shear instability if

$$We_\delta\left(\frac{\rho_2}{\rho_1}\right)\left(\frac{D_1}{\delta}\right)^3 >> 1, \qquad \text{with} \qquad We_\delta = \frac{\rho_2 U_2^2 \delta}{\gamma} \tag{38}$$

where D_1 is the diameter of the liquid nozzle. Condition in (38) is satisfied by all points in the database.

Table 1 Experimental datasets used in this investigation.

	Source	N^o of points	Fluids	Configuration	Data measured
Set 1	Raynal *et al*.	68	air-water	planar	wave frequency
Set 2	Marmottant & Villermaux	76	air-water	axisymmetric	wave frequency
Set 3	Marmottant & Villermaux	20	air-water	axisymmetric	wavelength
	Varga *et al*.	5			

Table 2 Fluid properties used for the predictions of the present model.

Fluid	Density (kg / m^3)	Dynamic viscosity (Pa.s)	Surface tension (N/m)
Air	1.2	1.8×10^{-5}	-
Water	998	1.0×10^{-3}	7.0×10^{-2}
Glycerine	1257	7.8×10^{-1}	6.3×10^{-2}

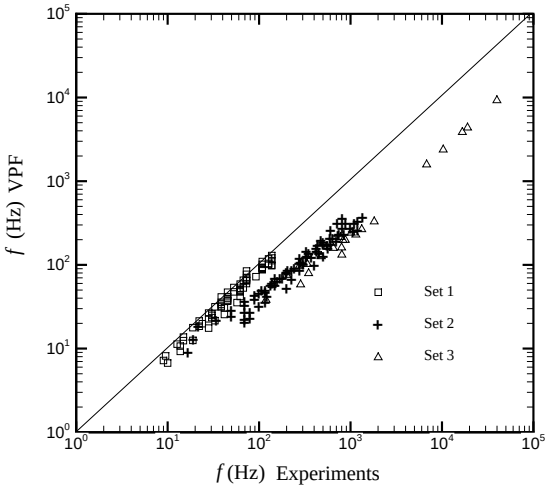

(a) VPF vs Experiments (air-water).

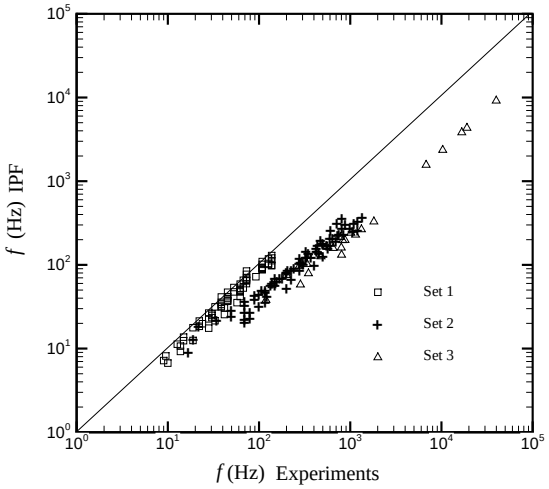

(b) IPF vs Experiments (air-water).

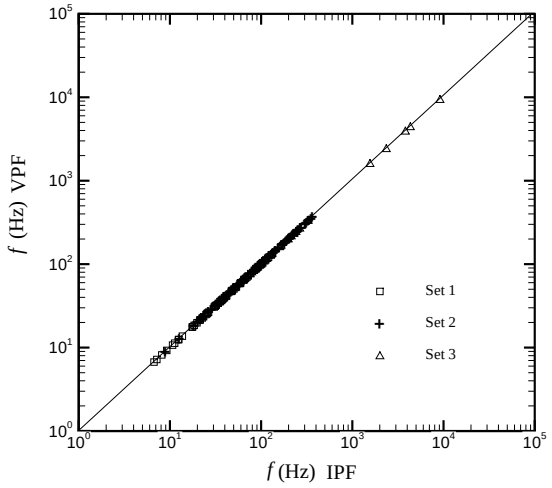

(c) VPF vs IPF (air-water).

Figure 6 Comparison of results for interfacial wave frequency for air-water: (a) VPF vs. experimental results; (b) IPF vs. experimental results, and (c) VPF vs. IPF. These plots show that VPF and IPF predictions give rise to similar results for air-water. VPF and IPF generate results in close agreement with the experimental data for the planar dataset (Set 1), whereas under-predict the experimental values for the axisymmetric sets (Sets 2 and 3). These trends suggest that a model that considers a cylindrical jet may be useful.

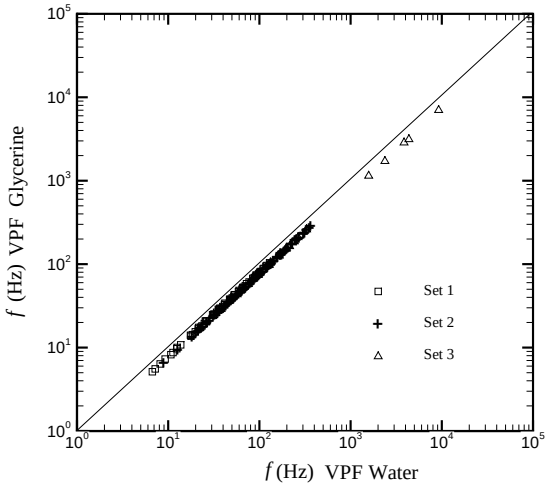

(a) VPF air-glycerine vs. air-water.

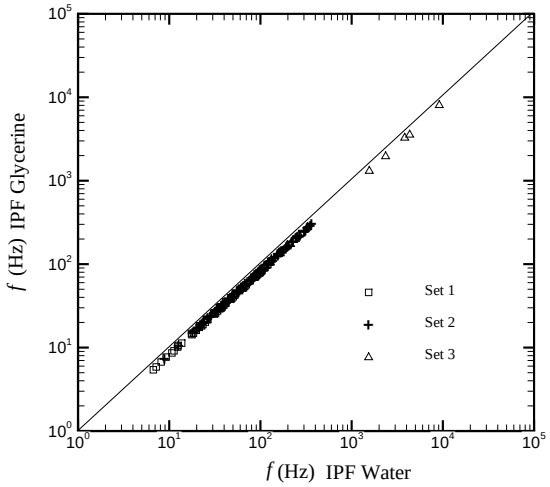

(b) IPF air-glycerine vs. air-water

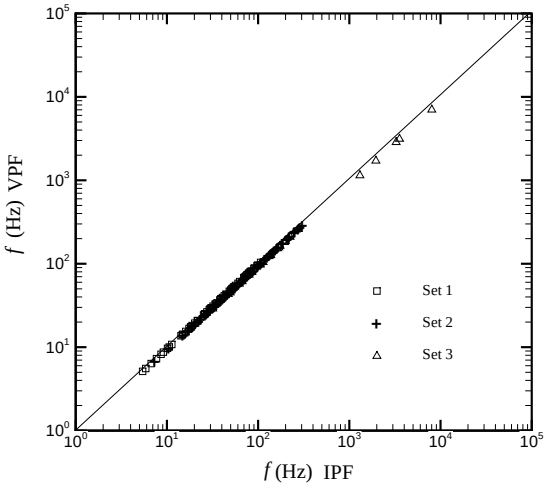

(c) VPF vs IPF (air-glycerine)

Figure 7 Comparison of results for interfacial wave frequency for air-glycerine and air-water: (a) VPF predictions; (b) IPF predictions, and (c) VPF vs. IPF for air-glycerine. Finite values of We_2 are considered. VPF predictions do not show significant differences with IPF results when water is replaced by a more viscous liquid as glycerine. This trend is confirmed in (c) where predictions from VPF and IPF are compared in the same plot.

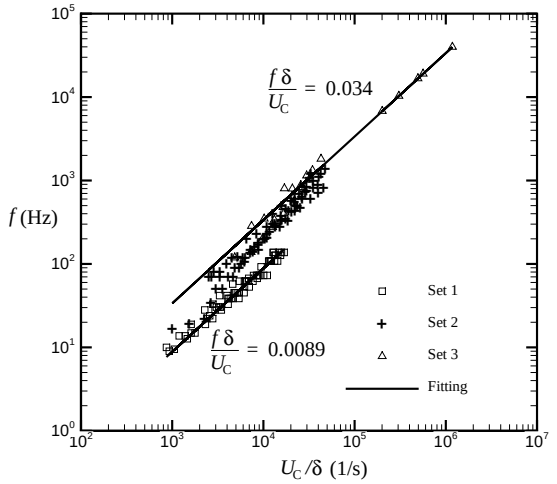

(a) Experimental data

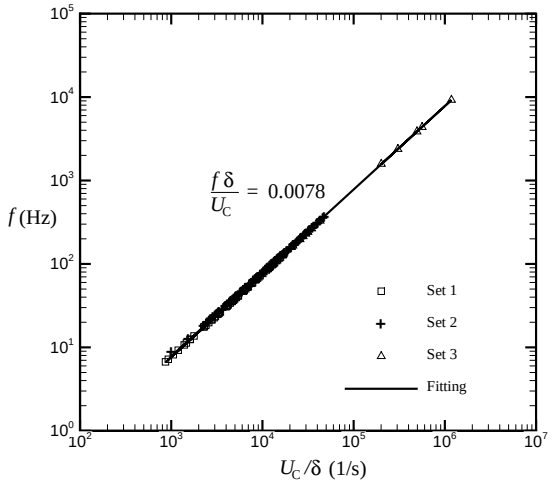

(b) VPF

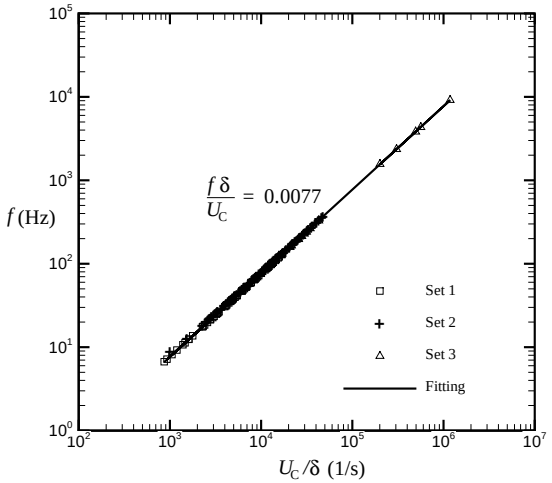

(c) IPF

Figure 8 Interfacial wave frequency as a function of the ratio U_C / δ for air-water: (a) Experimental data; (b) predictions from VPF and (c) predictions from IPF. The theoretical predictions consider finite We_2 defined from the fluid properties and flow rates for every experimental point. Linear models with zero intercept are fitted to both the experimental data corresponding to the planar motion (Set 1) and the data for the axisymmetric case (Sets 2 and 3). For VPF and IPF, linear models with zero intercept are fitted to the predictions corresponding to the entire dataset (Sets 1, 2 and 3). The planar data fitting in (a), $f = 0.0089U_C/\delta$, shows close agreement with the fitting obtained by Raynal *et al.* (1997), $f = 0.0087U_C/\delta$. Differences are attributed to the human factor acting in the process of data extraction from figures in the original work to tables in this study. Experimental data in (a) corresponding to axisymmetric experiments (Sets 2 and 3) follow a different trend as compared with the planar case. A similar behavior was

observed by Raynal *et al*. using data recorded from axisymmetric experiments (this data is not included in this work since the dependence of δ on Re_2 was not reported in the original work). Results in (b) from VPF and (c) from IPF are in close agreement with the experimental results for the planar dataset. The VPF and IPF approaches utilized in this investigation consider the planar configuration. In addition, VPF and IPF prediction fittings are almost the same (about 1% difference), as observed in (b) and (c).

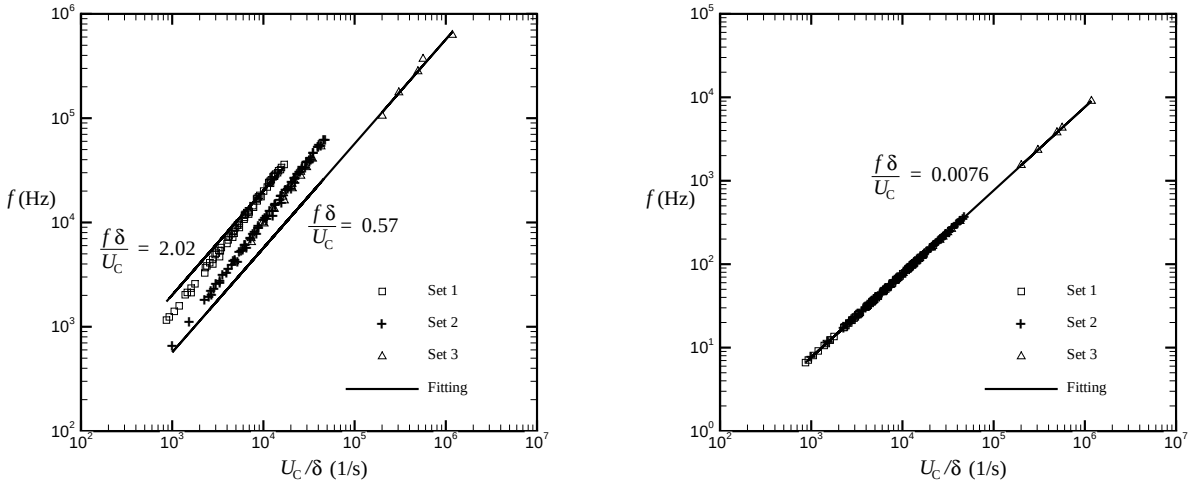

(a) VPF (infinite We_2) (b) IPF (infinite We_2)

Figure 9 Interfacial wave frequency as a function of the ratio U_C / δ for air-water: (a) predictions from VPF and (b) predictions from IPF. The theoretical predictions consider infinite We_2; therefore, surface tension effects are neglected. For VPF, linear models with zero intercept are fitted to both the predictions corresponding to the planar motion (Set 1) and the predictions for the axisymmetric case (Sets 2 and 3). IPF predicts $f \propto U_C / \delta$ for the entire set of points (the reader may inspect the dispersion relation with no surface tension effects (29)). The predictions from VPF in (a) show strong discrepancy with the results presented in Figure 8 (b) when finite We_2 is considered. This trend can be traced back to the results described in Figure 5, where VPF model predicts shorter "most dangerous" waves when We_2 tends to infinity than the inviscid results. Figures 8 (b) and 9 (a) indicate that surface tension effects should not be neglected when using VPF model. The trendline from IPF in (b) agrees with the corresponding fitting line obtained by Raynal *et al*. (1997) as expected since these authors used an inviscid approach to the stability problem neglecting surface tension effects. As represented in Figure 3, inviscid theory is not sensitive to changes in We_2, at least in the interval considered in this investigation.

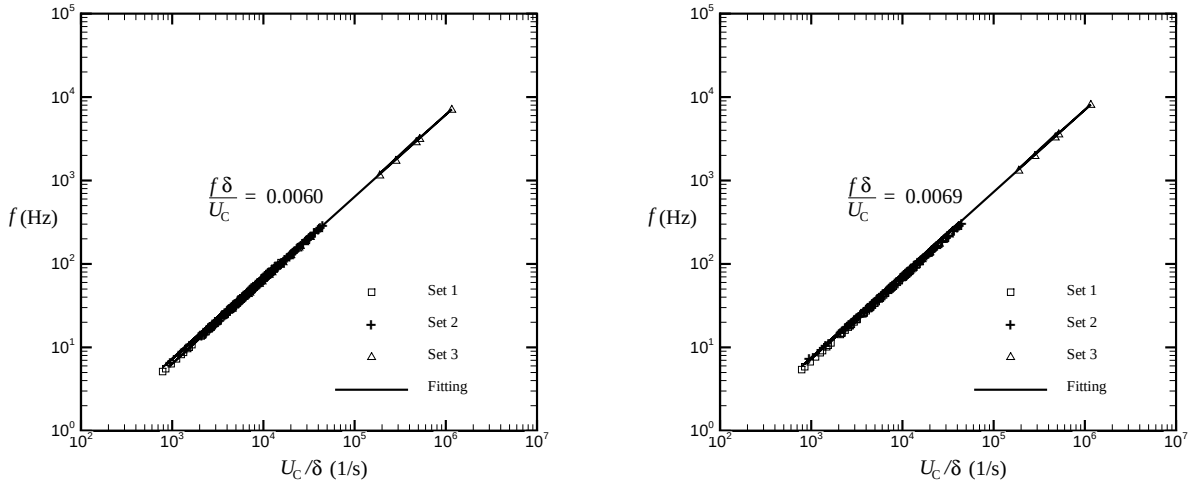

(a) VPF (air-glycerine) (b) IPF (air-glycerine)

Figure 10 Interfacial wave frequency as a function of the ratio U_C / δ for (a) predictions from VPF and (b) predictions from IPF when the properties of water are replaced by those of glycerine (density, viscosity and surface tension – see Table 2), keeping the same gas and liquid velocities. The theoretical predictions consider finite We_2; defined from the fluid properties (air-glycerine) and flow rates for every experimental point. Linear models with zero intercept are fitted to the predictions corresponding to the entire set of points. The difference observed between the fittings for VPF and IPF is about 13 %. For air-water this difference was 1%.

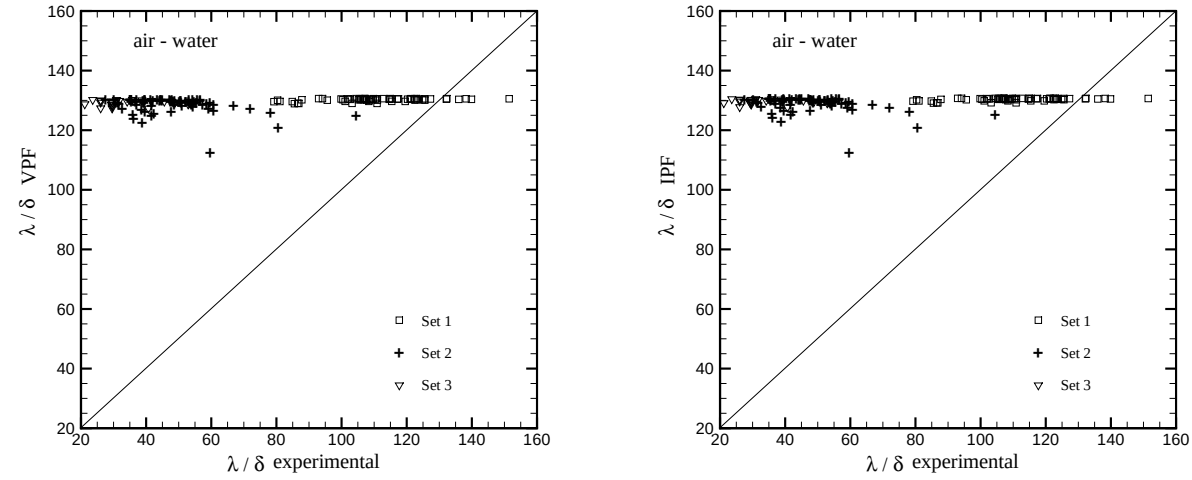

(a) VPF (infinite We_2) (b) IPF (infinite We_2)

Figure 11 Comparison of the dimensionless wavelength from VPF and IPF with experimental results for air-water. The experimental values for Set 1 (planar experiment)

tend to be closer to the 45^o line than the experimental values from Sets 2 and 3 (axysimmetric experiments).

Remark on Figures 8 and 11:

Marmottant & Villermaux (2004) attributed the discrepancies between experiments and theory to the assumption of a piecewise velocity profile. They argued that "the vorticity is not constant in the experimental boundary layer, contrary to the linear profile used in the stability analysis. The effective linear boundary-layer thickness to use in a prediction that matches experimental results is 4 to 6 times larger. This is consistent with the fact that experimental profiles are smoother than a broken line profile." The validity of this assertion may be questioned in light of the close agreement between theory and experiments for the planar case in terms of the wave frequency *f*.

If we define the quantity

$$\alpha = \frac{f\delta}{U_c}, \tag{39}$$

Then the ratio $\alpha_{\text{exp}} / \alpha_{\text{theo}}$ = 4.4 for the axisymmetric case (Sets 2 & 3) while equals 1.2 for the planar case (Set 1). For the axisymmetric data of Marmottant & Villermaux (Set 2 only) a ratio of about 3.0 is found, which coincides with the value reported in their work.

References

Bernal, L.P. & Roshko, A. (1986) Streamwise vortex structure in plane mixing layers. J. Fluid. Mech., **170**, 499 – 525.

Betchov, R. & Szewczyk, A. (1963) Stability of a shear layer between parallel streams. *Phys. Fluids* **6**, 1391-1396.

Criminale, W. O.: Jackson, T. L., and Joslin, R. D. (2003) *Theory and Computation of Hydrodynamic Stability*. Cambridge University Press.

Dimotakis, P.E. (1986) Two-dimensional shear layer entrainment. *AIAA J*. **24**, 1791 – 1796.

Drazin, P.G. and Reid, W.H. (1981) *Hydrodynamic Stability*. Cambridge University Press.

Marmottant, P. & Villermaux, E. (2004) On spray formation. *J. Fluid Mech*. **498**, 73 – 111.

Rayleigh, Lord. (1894) *The Theory of Sound*, 2nd. edition. London: Macmillan.

Raynal, L., Villermaux, E., Lasheras, J. & Hopfinger, E. (1997) Primary instability in liquid gas shear layers. In *11th Symp. on Turbulent Shear Flows* **3**, 27.1-27.5.

Varga, C.M., Lasheras, J.C. & Hopfinger, E.J. (2003) Initial breakup of a small-diameter liquid jet by a high-speed gas stream. *J. Fluid Mech*. **497**, 405 – 434.

Villermaux, E. (1998a) Mixing and spray formation in coaxial jets. *J. of Propulsion and Power* **14**, 807-817.

Villermaux, E. (1998b) On the role of viscosity in shear instabilities. *Phys. Fluids* **10**, 368-373.